



# **METHODS AND RESOURCES**

# Early regulation and alternative splicing dynamics in glucocorticoid muscle atrophy revealed by temporal omics in C2C12 myotubes

© Suzuka Nakagawa,<sup>1,2</sup> Aristotelis Misios,<sup>1</sup> © Oliver Popp,<sup>1</sup> © Philipp Mertins,<sup>1,3</sup> © Ernst Jarosch,<sup>1</sup> © Jens Fielitz,<sup>4,5</sup> and © Thomas Sommer<sup>2,6,7</sup>

<sup>1</sup>Max Delbrück Center for Molecular Medicine in the Helmholtz Association, Berlin, Germany; <sup>2</sup>Institute for Biology, Humboldt-University zu Berlin, Germany; <sup>3</sup>Berlin Institute of Health, Berlin, Germany; <sup>4</sup>DZHK (German Center for Cardiovascular Research), Partner Site Berlin, Berlin, Germany; <sup>5</sup>DZHK (German Center for Cardiovascular Research), Partner Site Greifswald, Germany; <sup>6</sup>Department of Internal Medicine B, Cardiology, University Medicine Greifswald, Greifswald, Germany; and <sup>7</sup>Institute for Biomedical Translation Lower Saxony, Hannover, Germany

#### **Abstract**

Skeletal muscle atrophy and weakness are major contributors to morbidity, prolonged recovery, and long-term disability across a wide range of diseases. Atrophy is caused by the breakdown of sarcomeric proteins, resulting in loss of muscle mass and strength. Molecular mechanisms underlying the onset of muscle atrophy and its progression have been analyzed in patients, mice, and cell culture, but the complementarity of these model systems remains to be explored. Here, we applied deep coverage transcriptomic and proteomic profiling for an updated view on dynamic changes during dexamethasone-induced atrophy in the widely used murine skeletal muscle cell line C2C12. Comparison with published mouse data confirmed that muscle differentiation is well recapitulated in C2C12 myotubes. Under dexamethasone treatment, this model was particularly suited to capture early atrophy events. We additionally identified alterations in mitochondrial gene expression and differential alternative splicing events during early-stage myotube atrophy. This dataset complements existing in vivo data and provides novel insights into the regulatory processes during skeletal muscle wasting.

**NEW & NOTEWORTHY** Skeletal muscle atrophy studies rely on in vivo mouse data as well as in vitro data. Our deep coverage transcriptome and proteome data reveal that the commonly used C2C12 cells faithfully recapitulate differentiation and atrophy markers, with significant alternative splicing occurring under dexamethasone atrophy. Using published mouse tissue data of comparable methods, we provide an up-to-date resource for skeletal muscle atrophy to complement animal studies.

alternative splicing; atrophy; glucocorticoid; omics; skeletal muscle

# INTRODUCTION

Skeletal muscle atrophy is a condition that severely impacts patients' quality of life by reducing muscle mass and strength. Research into mechanisms of atrophy onset and progression provides identification of critical factors whose activity may be modified to delay or reverse muscle wasting and ultimately promote recovery of patients. Atrophy is tightly associated with proteolytic systems like the ubiquitin proteasome system (UPS) and the autophagy lysosome pathway that are known to mediate degradation of sarcomeric proteins (1, 2). Although several proteins termed atrogenes have been identified as specifically associated with striated muscle atrophy (e.g., Fbxo32/MAFbx/ Atrogin-1, Trim63/MuRF1, Fbxo30/MUSA 1, Fbxo21/SMART, and Trim32) (3–5), a robust mechanism of how they contribute to the disassembly of sarcomeres or degradation of their constituents is still under investigation. Moreover, transcriptional and translational processes that initiate, accelerate, or prevent degradation of sarcomere components are still obscure.

Conventional research on skeletal muscle atrophy mostly relies on results obtained from mouse models and is complemented by various muscle cell lines. Immortalized murine C2C12 myoblasts are capable of differentiating into multinuclear bodies (myotubes) with the formation of sarcomeres. These cells can then be used to further induce myotube atrophy by using various stimuli, such as the synthetic glucocorticoid dexamethasone (dex). Glucocorticoids (GCs) bind to glucocorticoid receptors (GRs) to allow nuclear translocation of the GR complex. Within the nucleus, the GR complex upregulates expression of FoxO transcription factors to transcribe atrogenes, such as MAFbx/Atrogin-1 and MuRF1 (3, 6, 7). In clinical settings, prolonged or high-dosage administration of GCs, for example, to counter inflammation by inhibiting the NF-kB pathway, can trigger muscle atrophy and induce degradation of sarcomeric proteins (8-10). Despite this, GCs are used as the standard of care for patients with Duchenne's muscular dystrophy, where long-term administration of GCs significantly delays reaching disease milestones





due to its anti-inflammatory and contractility-enhancing properties (11, 12).

Skeletal muscle differentiation, senescence, regeneration, and disease states are best studied in tissues where myofibrils containing myotube bundles are exposed to a multitude of endocrine and metabolic signals from surrounding skeletal, neural, and vascular structures. Several mRNA and protein datasets have been published for murine or rat muscle tissue, describing molecular changes in atrophy. Most of these studies focus on one particular atrophy model with a single screening technique (13–15), whereas others cross-compare multiple atrophy models, such as sarcopenia, cancer cachexia, and dex-induced atrophy with protein and RNA data (16, 17). Abdelmoez et al. (18) published a cross-comparative analysis of published transcriptomic datasets from mouse (C2C12), rat (L6), and human skeletal muscle cell lines, albeit without atrophy stimuli. The heterogeneity in experimental setups for muscle studies is known to give a high variability in results, which are difficult to compare (19). Thus, a comprehensive dataset obtained from a commonly used cell line, which has lower biological heterogeneity compared with animals, is cost-efficient, and is permissive to extensive protocol optimization, would provide valuable information for atrophy studies in animals. In addition, comparison with the published mouse dataset of the same atrophy stimulus would highlight the biological relevance and limitation of these models.

Here, we present a matched time course dataset of deep mRNA and whole proteome coverage of C2C12 myotubes treated with dex. Our results give information on cellular events during myoblast-to-myotube differentiation, with strong reproducibility of observations previously seen in mice. Furthermore, our data appear to portray relatively early events following dex exposure, with insights into cellular activities preceding sarcomeric breakdown. We expect this resource to provide new perspectives on atrophy to better design and interpret future skeletal muscle studies by highlighting characteristics specific to C2C12 cells.

# **MATERIALS AND METHODS**

#### **Cell Culture and Dexamethasone-Induced Atrophy**

C2C12 cells (ATCC CRL1722) were cultured in growth medium [10% fetal bovine serum (FBS); Gibco, 10270-106], 1% penicillin/streptomycin (P/S; Sigma-Aldrich), high glucose Dulbecco's modified Eagle's medium (DMEM; Sigma-Aldrich) and maintained at 50%-60% confluency. For differentiation, cells were switched to differentiation medium (DM. 2% FBS, 1% P/S, high-glucose DMEM) once they reached 80%-90% confluency (considered day 0) and cultured for 7 days with fresh DM supplied every 2-3 days. To induce atrophy, cells were treated with 100 µM dexamethasone (Sigma-Aldrich) or an equivalent dilution of 99.99% ethanol (Sigma-Aldrich) in DM and cultured for up to three more days. Replicates were prepared from various passages and stocks and cultured in a staggered manner to be considered biological replicates. Mycoplasma presence was checked intermittently using the LookOut Mycoplasma Detection PCR kit (Sigma-Aldrich).

## **RNA Extraction and Quality Control**

Total RNA was extracted using Zymo Direct-zol RNA Miniprep Plus (ZymoResearch) according to the manufacturer's instructions. On collection days, cells were washed twice with D-PBS (Sigma-Aldrich) and then lysed with the supplied lysis buffer for 5 min at room temperature before collection with a cell scraper. Samples were snap frozen and stored at -80°C until extraction. Samples were thawed on ice, and total RNA was extracted with all centrifugation steps performed at 20,817 g and an additional empty centrifugation step before elution. RNA was eluted using the supplied nuclease-free double-distilled water. An aliquot was taken to measure A260/280 and A260/230 on a NanoDrop2000 (Thermo Scientific, Peqlab Biotechnologie GmbH). Ratios >1.9 for both measurements were deemed as contamination-free. Where samples did not pass these criteria, RNA was precipitated using ethanol and resuspended in nuclease-free water. RNA integrity was checked using BioAnalyzer 2000 and the RNA 6000 Nano kit with the RNA 6000 ladder (Agilent). A RNA integrity number (RIN) score of >8.0 was chosen as the passing score for subsequent library preparation using the TruSeq Stranded mRNA kit (Illumina) according to the manufacturer's instructions.

## **Bulk RNA Sequencing**

RNA sequencing was performed using the NovaSeq 6000 at the MDC Genomics Technology Platform. Samples were sequenced in S1 mode using paired-end sequencing with  $2 \times 100$  bp read length and dual indexing. Samples were demultiplexed and read length quantified using Salmon via pseudoalignment against all transcripts and on reference chromosomes in the gencode vM12 mouse transcriptome annotations using parameters: "salmon quant – I ISR – segBias – gcBias – validateMappings." RNA-just seq fold-changes were calculated using the tximport package with default settings for isoform-aware quantification and DEseq (SCR\_000154).

# **Differential Alternative Splicing and Isoform Switch** Analysis

All computational analyses were performed using R (v. 4.4.1) and relevant packages as described: Raw RNA-Seq reads were pseudo-aligned and quantified using Kallisto (v. 0.51.1, SCR\_016582) with the mouse reference transcriptome corresponding to genome assembly GRCm39. The resulting transcript-level abundance estimates [transcripts per million (TPM) and estimated counts] were imported into R using the importIsoformExpression() function from the IsoformSwitchAnalyzeR package (v. 2.6.0, SCR\_027320). Isoform-level analysis was also conducted using IsoformSwitchAnalyzeR. A switchAnalyzeRlist object was created from Kallisto outputs. Isoform switches were identified between conditions and potential functional consequences of switching events. The default thresholds of isoform\_switch\_q\_value < 0.05 and differential isoform fraction abs (dIF) > 0.1 were used unless otherwise stated. For the comparison with the differentially expressed genes, a threshold of P-adjusted value  $P_{\rm adj} < 0.05$  was used.

# **Tandem Mass Tag Mass Spectrometry Sample Preparation**

On collection days, cells were washed three times with phosphate-buffered saline (PBS), scraped with 1 mL D-PBS into a 1.5-mL microcentrifuge tube, and centrifuged at 500 g for 3 min at 4°C. The supernatant was discarded, and the cell pellet was snap frozen in liquid nitrogen before storage at -80°C. For protein extraction, cell pellets were lysed in 8 M urea lysis buffer containing 75 mM NaCl, 50 mM Tris-HCl (pH 8.0), 1 mM EDTA, 2 μg/mL aprotinin, 10 μg/mL leupeptin, 1 mM PMSF, 1:100 (vol/vol) phosphatase inhibitor cocktail 2, 1:100 (vol/vol) phosphatase inhibitor cocktail 3, 10 mM NaF, and 20 µM PUGNAc. Lysates were sonicated on ice using a probe sonicator at 20% amplitude in three cycles of 10 s on and 20 s off. Insoluble debris was removed by centrifugation at 14,000 g for 10 min at 4°C. Protein concentration was determined using the bicinchoninic acid protein assay kit (Pierce, Thermo Fisher Scientific) according to the manufacturer's instructions.

## **TMT Labeling and Peptide Digestion**

For each sample, 1 mg of protein was reduced with 5 mM dithiothreitol (DTT) at 37°C for 45 min, alkylated with 15 mM iodoacetamide in the dark for 30 min at room temperature, and quenched with 5 mM DTT for 15 min. Proteins were sequentially digested with Lys-C (1:100 enzyme-to-protein ratio) for 3 h at 37°C, followed by trypsin digestion (1:50 ratio) overnight at 37°C. Peptides were desalted using Sep-Pak C18 cartridges (Waters) and dried in a vacuum concentrator. Tandem Mass Tag (TMTpro) 16-plex labeling was performed using two sets of TMTpro reagents (Thermo Fisher Scientific) following the protocol described by Mertins et al. (20). Each TMT 16-plex experiment included a balanced representation of time points, with one channel designated for a pooled reference sample containing equal proportions of peptides from all other channels. Labeled samples were pooled, desalted, and fractionated using high-pH reversed-phase liquid chromatography on an UltiMate 3000 HPLC system (Thermo Scientific) equipped with an XBridge Peptide BEH C18 column (130 Å, 3.5  $\mu$ m, 4.6 mm  $\times$  250 mm; Waters). Peptides were separated into 24 concatenated fractions.

# **Liquid Chromatography-Tandem Mass Spectrometry Analysis**

Peptide fractions were resuspended in 0.1% formic acid and analyzed using an EASY-nLC 1200 system coupled to an Orbitrap Exploris 480 mass spectrometer (Thermo Fisher Scientific). Peptides were separated on a 50 cm  $\times$  75  $\mu$ m inner diameter EASY-Spray column (Thermo Fisher Scientific) packed with 1.9 µm C18 beads (PepMap RSLC). A 110 min HPLC gradient was applied at a flow rate of 250 nL/min. Data acquisition was performed in data-dependent acquisition mode, with mass spectroscopy (MS)/MS spectra collected at a resolution of 45,000 and an isolation width of 0.4 mass-tocharge ratio.

## **Analysis of TMT-MS Data**

Raw data files were processed using MaxQuant (v.1.6.10.43, SCR\_014485) and searched against the *Mus musculus* proteome

(2018-07) downloaded from UniProt, including isoforms. Trypsin/Lys-C was specified as the digestion enzyme, with up to two missed cleavages allowed. Carbamidomethylation of cysteine was set as a fixed modification, whereas oxidation of methionine and acetylation of protein N-termini were specified as variable modifications. A precursor ion fraction (PIF) filter of 0.5 was applied. Peptide-spectrum matches and protein identifications were filtered at a false discovery rate of 1%. Only proteins with at least two unique peptides and valid reporter ion intensities across all samples were retained for further analysis.

Protein abundances were calculated from log<sub>2</sub>-transformed, corrected TMT reporter ion intensities. Intensities were normalized against the internal reference, followed by sample-wise median-median absolute deviation (MAD) normalization to correct for systematic variations. Differential protein expression analysis was performed using the limma R package (SCR\_010943) (21), with Benjamini-Hochberg correction applied for multiple testing. Gene lists belonging to the indicated gene ontology (GO) terms were retrieved from the Mouse Genome Database, Mouse Genome Informatics, The Jackson Laboratory, Bar Harbor, Maine (http://www.informatics.jax.org).

# Gene Set Enrichment Analysis, GO Enrichment, and **Protein-Protein Interaction Enrichment Analysis**

For gene set enrichment analysis (GSEA) of RNA data, DESeq2 (SCR\_015687)-generated pairwise comparison data was enriched using clusterProfiler [v. 4.14.6, SCR\_016884 (22)] and the DOSE package [v. 4.0.1 (23)]. Gene lists for significantly increased and decreased proteins were generated using  $P_{\rm adi}$  value  $\leq 0.05$  and/or  $-0.6 \leq \log FC \leq 1$  from our TMT-MS data to account for fold-change by 50%. Proteinprotein interaction enrichment analysis was then performed using Metascape (24) and visualized in Cytoscape (25). GO enrichment for protein data was performed using string.db (v. 12.0) (22).

# RT-qPCR

Aliquots of total RNA isolated for the bulk RNA sequencing were used to validate relative changes in the quantity of certain transcripts. Total RNA (1 µg) was reverse transcribed into cDNA using Maxima H Minus (VWR Technologies) and oligo-dT<sub>20</sub> primer per reaction. Total RNA was incubated with 10 mM dNTPs at 65°C for 5 min, then briefly placed on ice. A mix of  $5 \times RT$  buffer provided with Maxima H Minus was mixed with RiboLock RNase Inhibitor (20 U per reaction, Life Technologies) and added before incubation at 50°C for 30 min. The cDNA mixture was then diluted 1:20 using nuclease-free water (Promega).

Bio-Rad CFX96 was used to quantify SYBR Green-mediated amplification signals. In a 96-well plate (Biozym), cDNA was pipetted with RT-qPCR primers and 2× GoTaq qPCR master mix (Promega). A water blank was used to check for primer-primer dimer formation. Plates were cycled as follows: 95°C for 2 min, 41× loops of 95°C for 3 s, 62°C for 30 s, ending with a 60°C-90°C temperature gradient of 1°C increment. Plates were read after the 62°C annealing step and again after the temperature gradient. Signals were calculated using the  $2^{-\Delta\Delta Ct}$  method with more

Table 1. List of primers used

	RT-qPCR F	RT-qPCR Primers	
Target	Forward (3'-5')	Reverse (3'-5')	
B2M	CTGCTACGTAACACAGTTCCACCC	CATGATGCTTGATCACATGTCTCG	
Fbxo30	GAGAAGCCAGGGTTTGAGC	TCATACAGTGTGAGTGCTGCTG	
Fbxo32	GGGGGAAGCTTTCAACAG	TGAGGCCTTTGAAGGCAG	
Hprt	TCCCTGGTTAAGCAGTACAG	GCTTTGTATTTGGCTTTTCC	
Myf5	CTCCAACTGCTCTGACGGC	AGACGTGATCCGATCCACAAT	
Myog	CGATCTCCGCTACAGAGGC	GGACGTAAGGGAGTGCAGAT	
Trim63	ATTGTAGAAGCCTCCAAGGGC	CTTTACCCTCTGTGGTCACG	

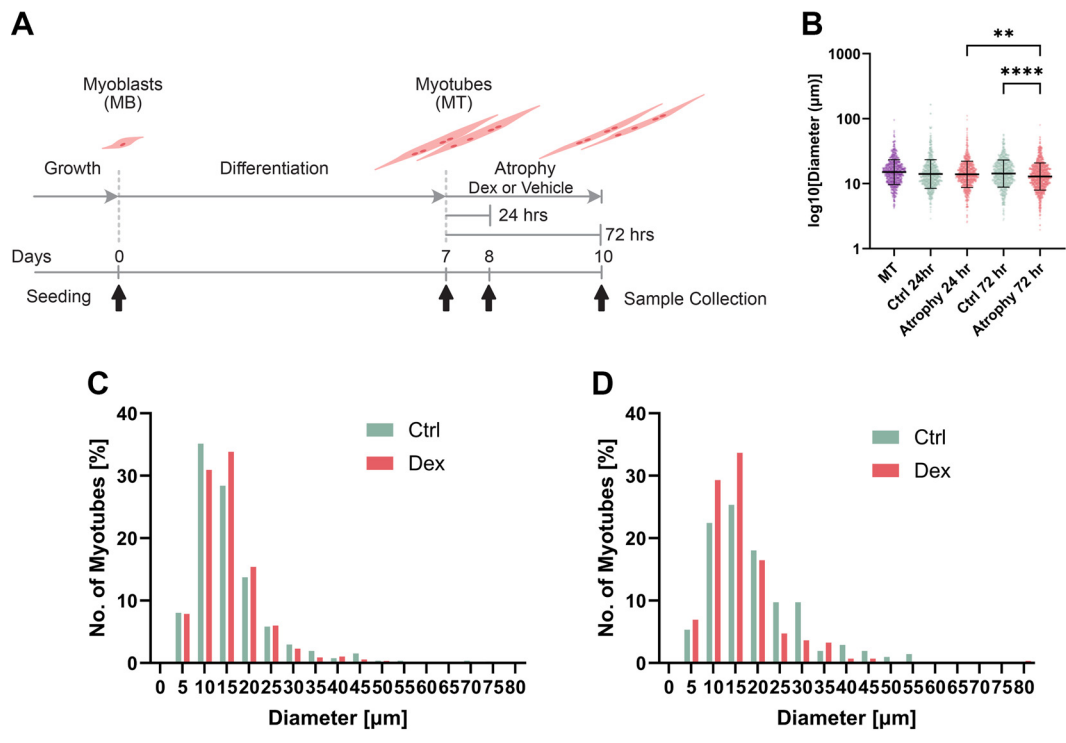
than one housekeeping gene. Primers used are listed in Table 1.

## Immunofluorescence, Fusion Index, and Diameter Measurements

Cells were cultured and treated for atrophy induction in ibiTreat 35 mm dishes (ibidi). On days matching the bulk RNA-Seg and TMT-MS samples, dishes were washed with D-PBS(-) and fixed with 4% PFA for 30 min at room temperature. Dishes were washed and permeabilized using 0.4% Triton X-100 0.5% BSA D-PBS(++) for 30 min at room temperature. Cells were then washed with 0.5% Tween-20 D-PBS(++) henceforth and blocked in 0.05% Triton-X100 3% BSA D-PBS(++) for >30 min. After washing, samples were incubated overnight with antibodies against fast/ type-II myosin heavy chain (MyHC; sigma, M4276, RRID:

AB\_477190) at 4°C. Following another wash, dishes were incubated with Cy5 goat anti-mouse (Invitrogen, A10524, RRID:AB\_10562712) at 2 µg/mL concentration in blocking buffer for 1 h at room temperature. Cells were washed again before incubation with Hoechst 33342 diluted to 1  $\mu$ g/mL in D-PBS(++) for 5 min at room temperature. Cells were washed and stored in D-PBS(++) and imaged on a Leica SP8 confocal microscope. All images were analyzed using Fiji (SCR\_002285) (26).

The fusion index was calculated as the number of nuclei inside a MyHC-positive cell out of the total number of nuclei in a field of view. Diameter measurements were carried out on MyHC-positive cells in the vehicle control or atrophy conditions. Statistical significance comparing the diameter of all conditions was carried out using the Kruskal-Wallis test.



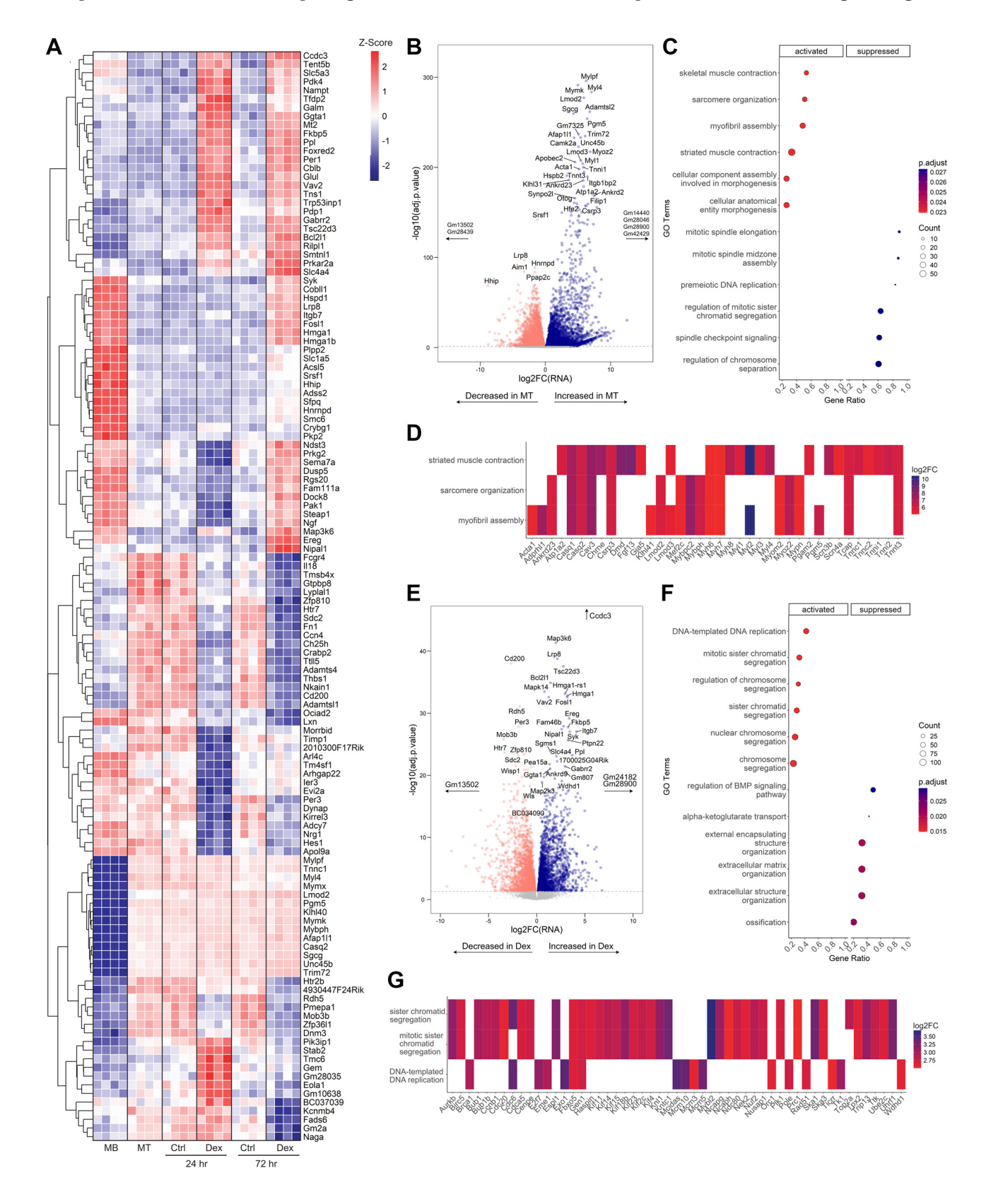
 $\textbf{Figure 1.} \ \ \text{Quantification of C2C12 morphology after 7 days of differentiation and treatment with 100 } \ \mu\text{M} \ \ dex. \ \textit{A: timeline schematic of sample collection}$ for RNA-Seq and TMT-MS data collection. C2C12 myoblasts (MB) were differentiated for 7 days into myotubes (MT), before switching to dexamethasone-containing (100 µM, dex) atrophy medium or solvent control (0.1% ethanol, vehicle). Arrows indicate days of sample collection. B: diameter measurements of fast skeletal MyHC-positive C2C12s at the indicated time points. Each data point indicates a diameter measurement. Five images were analyzed per biological replicate, n=3. Lines indicate geometric means  $\pm$  SD. Significance was assessed by a Kruskal–Wallis test. \*\* $P \le 0.01$ , \*\*\*\* $P \le 0.01$ 0.0001. C and D: no. of MyHC-positive C2C12s binned for indicated diameters at 24 h (C) and 72 h (D). Values are shown as % of total. Five images were analyzed per biological replicate, n = 3. MyHC, myosin heavy chain; TMT-MS, tandem mass tag mass spectrometry.

#### UV

# Data Exploration, Statistical Analyses, and Visualization

Data visualization and Student's moderated t test for RNA-Seq, differential alternative splicing (DAS), isoform

switch analyses, and TMT-MS data were performed using base R functions, ggplot2 (v. 3.5.1, SCR\_014601), and pheatmap (v. 1.0.12, SCR\_016418). Custom plots of gene expression, isoform expression, and isoform usage were generated





from processed data. Venn diagrams were plotted using the VennDiagram package (v. 1.7.3, SCR\_002414). Statistical testing and visualization of quantified immunofluorescence data for cell morphology were performed using GraphPad Prism 10 (v. 10.4.1, SCR\_002798).

## RESULTS

### Validation of the C2C12 Dexamethasone Atrophy Model

The aim of this study was to quantitate changes in RNA abundance and protein amounts across defined stages of C2C12 myoblast-to-myotube differentiation and subsequent dex-induced atrophy. Dex was chosen as the atrophy stimulus, as several disease states resulting in muscle atrophy (e.g., sepsis and acidosis) have higher levels of circulating endogenous GCs, and patients treated with dex in clinical settings display muscle atrophy, thus providing insight useful to multiple atrophy contexts (10, 27). Furthermore, dex can also be used in rodents to induce atrophy, allowing cross-comparison of cell lines to animals. To this end, myoblasts were differentiated into myotubes for 7 days, followed by treatment with 100 μM dex for 24 or 72 h to induce atrophy (Fig. 1A). A 7-day differentiation period was chosen based on literature as the longest commonly used differentiation for C2C12 cells (28, 29). The rationale was to 1) maximize the number of fully differentiated myotubes, 2) allow sufficient time for atrophy to occur while maintaining cell adherence, and 3) reduce the presence of undifferentiated myoblasts. Dex concentration was guided by published studies, followed by titration experiments (30-33). Final conditions were selected based on microscopic observations that revealed the most noticeable diameter loss after 24 and 72 h (data not shown).

We validated our C2C12 differentiation and atrophy model by assessing fusion indices across six conditions: undifferentiated myoblasts, day 7 myotubes, vehicle-treated controls at 24 and 72 h, and dex-treated samples after 24 and 72 h. Cells were fixed and stained with an anti-MyHC antibody, and fusion indices were calculated as the number of Hoechststained nuclei within MyHC-positive cells relative to the total nuclei per field of view. A significant increase of multinuclear cells was observed between myoblasts and all differentiated conditions (P value < 0.0001), with no significant differences among later time points (Supplemental Fig. S1A). These results confirm that the protocol reliably produces differentiated myotubes and that subsequent dex-treatment does not significantly alter the fusibility of these cells.

Dex-treatment of myotubes for 24 h led to a slight, statistically insignificant reduction in MyHC-positive cell diameter

compared with vehicle-treated controls (Fig. 1, B and C). After 72 h, diameter reduction became more pronounced, as indicated by a shift in geometric mean values (Fig. 1, B and D), consistent with the onset of atrophy. Further decrease between 24- and 72-h dex-treated samples supported a progressive atrophy phenotype (Supplemental Fig. S1B). In summary, this experimental setup reliably models C2C12 myoblast differentiation followed by dex-induced atrophy and was used to generate samples for next-generation bulk mRNA sequencing (RNA-Seq) to analyze changes in mRNA expression and splicing and mass spectrometry to quantitate differences in protein abundance.

# **Transcriptomic Analyses Reveal Tissue-Comparable Differentiation Hallmarks and Identifies Novel Putative Contributors of Atrophy**

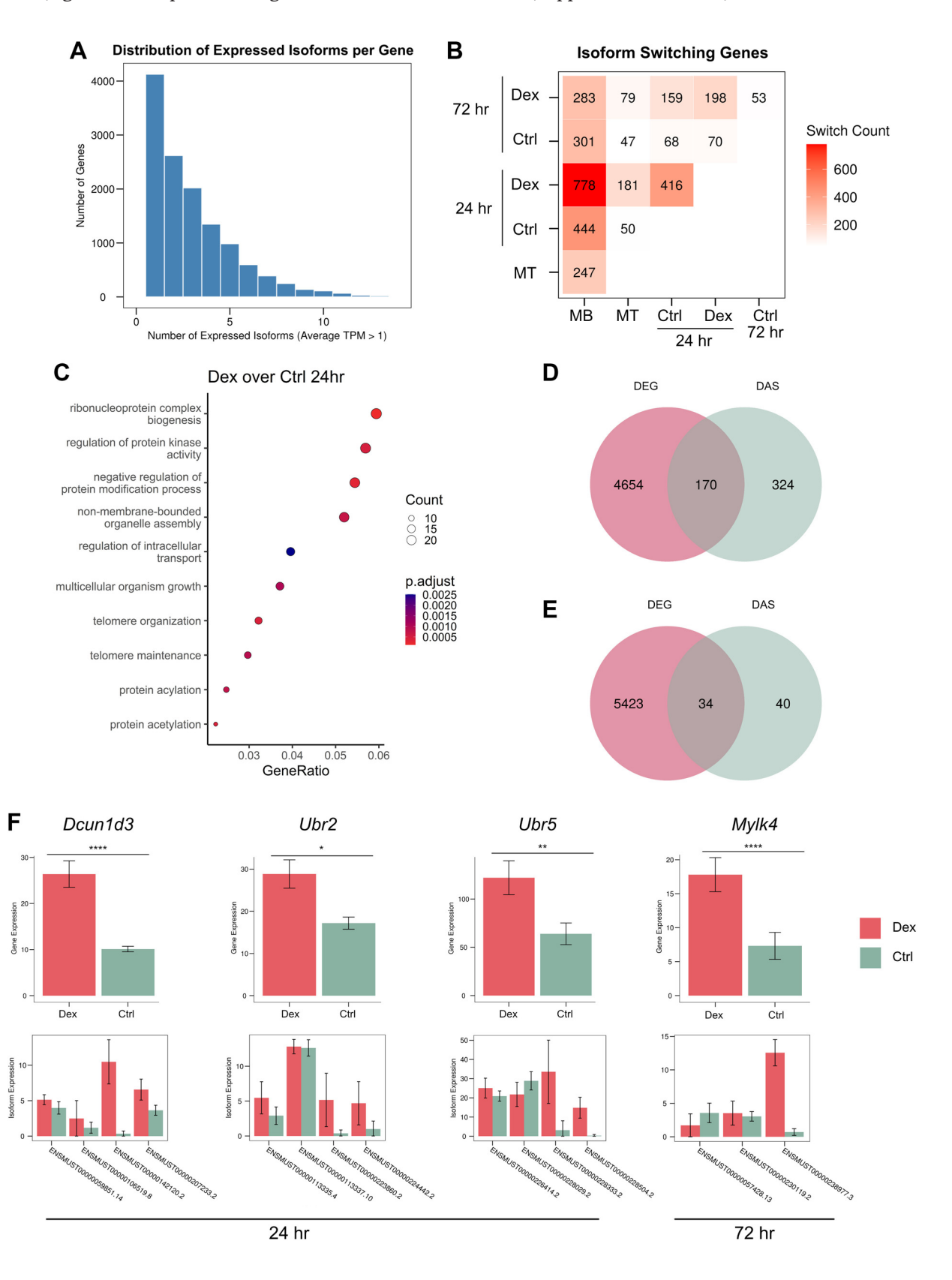
From our RNA-Seq efforts, we detected ~30,000 genes across all time points. Principal component analysis (PCA) revealed pronounced clustering of biological replicates for each condition, confirming the reproducibility of transcriptional states (Supplemental Fig. 1C). As an initial validation step, we quantitated the expression of known myogenic factors (Myf5 and Myog) (34, 35) and atrogenes (Trim63, Fbxo32, and Fbxo30) (3, 4) using RT-qPCR (Supplemental Fig. S1D). The expression patterns of these genes were consistent with published data (18, 29) and in agreement with our RNA-Seq results (Supplemental Fig. S1E). Notably, Fbxo30 showed differential expression only in RT-qPCR but not in RNA-Seq, likely reflecting differences in detection sensitivity. In general, this indicates that the quantification of our RNA-Seq data gave reliable information on actual transcriptional changes.

To characterize gene expression dynamics during differentiation and atrophy, RNA profiles from all postdifferentiated time points were compared pairwise to the myoblast condition ( $P_{adj}$  value  $\leq 0.05$ ) and visualized using normalized counts in a heat map (Fig. 2A). In myotubes, we observed significant upregulation of transcripts encoding myoblast fusion regulators [Myomaker/Mymk, Myomixer/ Mymx (36, 37)], key myogenic regulators (Klhl40/Klhl40), and striated muscle-specific chaperones involved in sarcomere organization [Unc45b/Unc45b (38)]. In addition, we detected increased expression of the Ca<sup>2+</sup>-binding protein Troponin C (Tnnc1), the ubiquitin E3 ligase Trim72 that negatively regulates differentiation (39), and Camk2a involved in  $Ca^{2+}$  signaling (40) (Fig. 2, A and B). Gene set enrichment analysis (GSEA) further revealed upregulation of pathways related to skeletal muscle contraction, sarcomere organization, and myofibril assembly (GO:0003009, GO:0045214,

Figure 2. Bulk RNA-Seq reveals expression of differentiation and atrophy markers. A: Z-score heat map of normalized transcript counts of top 15 significantly changing genes ( $P_{adj}$  value  $\leq$  0.05) from comparisons of MB vs. MT, Dex vs. Ctrl 24 h, Dex vs. Ctrl 72 h, and Dex 24 h vs. Dex 72 h. Euclidean clusters of MB vs. MT, Dex vs. Ctrl 24 h, Dex vs. Ctrl 72 h, and Dex 24 h vs. Dex 72 h. Euclidean clusters of MB vs. MT, Dex vs. Ctrl 24 h, Dex vs. Ctrl 72 h, and Dex 24 h vs. Dex 72 h. Euclidean clusters of MB vs. MT, Dex vs. Ctrl 24 h, Dex vs. Ctrl 72 h, and Dex 24 h vs. Dex 72 h. Euclidean clusters of MB vs. MT, Dex vs. Ctrl 24 h, Dex vs. Ctrl 72 h, and Dex 24 h vs. Dex 72 h. Euclidean clusters of MB vs. MT, Dex vs. Ctrl 24 h, Dex vs. Ctrl 72 h, and Dex 24 h vs. Dex 72 h. Euclidean clusters of MB vs. MT, Dex vs. Ctrl 72 h, Dex vs. Ctrl 72 h, and Dex 24 h vs. Dex 72 h. Euclidean clusters of MB vs. MT, Dex vs. Ctrl 72 h, Dex vs. Ctrl 72 h, and Dex 24 h vs. Dex 72 h. Euclidean clusters of MB vs. MT, Dex vs. Ctrl 72 h, Dex vs. Ctrl 72 h, and Dex 24 h vs. Dex 72 h. Euclidean clusters of MB vs. MT, Dex vs. Ctrl 72 h, Dex vs. Ctrl 72 h, and Dex 24 h vs. Dex 72 h. Euclidean clusters of MB vs. MT, Dex vs. Ctrl 72 h, Dex vs. Ctrl 72 h, and Dex 24 h vs. Dex 72 h. Euclidean clusters of MB vs. MT, Dex vs. Ctrl 72 h, Dex vs. Ctrl 72 h, and Dex 24 h vs. Dex 72 h. Euclidean clusters of MB vs. MT, Dex vs. Ctrl 72 h, Dex vs. Ctrl 72 h, and Dex 24 h vs. Dex 72 h. Euclidean clusters of MB vs. MT, Dex vs. Ctrl 72 h, Dex vs. Ctrl 72 h, and Dex 24 h vs. Dex 72 h. Euclidean clusters of MB vs. MT, Dex vs. Ctrl 72 h, and Dex 24 h vs. Dex 72 h. Euclidean clusters of MB vs. MT, Dex vs. Ctrl 72 h, and Dex vs. Ctrl 74 h, tering was applied row-wise. Each square corresponds to a biological replicate data point. Significance testing using a moderated t test. B: volcano plot  $of log_2 Fold Change in transcript plotted against -log10 (\textit{P}_{adj} \ value) for \ MT \ (\textit{right}, blue) against \ MB \ (\textit{left}, pink). The gray dashed line indicates \textit{P}_{adj} \ value = 1000 \ value) for \ MT \ (\textit{right}, blue) against \ MB \ (\textit{left}, pink). The gray dashed line indicates \textit{P}_{adj} \ value = 1000 \ value) for \ MT \ (\textit{right}, blue) against \ MB \ (\textit{left}, pink). The gray dashed line indicates \textit{P}_{adj} \ value) for \ MT \ (\textit{right}, blue) against \ MB \ (\textit{left}, pink). The gray dashed line indicates \textit{P}_{adj} \ value) for \ MT \ (\textit{right}, blue) against \ MB \ (\textit{left}, pink) agains$ 0.05. Significance testing using a moderated t test. C: GSEA analysis of enriched biological pathways in MT compared with MB using cluster Profiler. D: plot of genes belonging to the top three activated biological processes from C. Colors correspond to the log<sub>2</sub>FoldChanges (log<sub>2</sub>FC) in normalized  $counts \ of \ transcripts. \ Only \ genes \ with \ log_2FC \geq 6 \ are \ shown. \ \textit{E}: \ volcano \ plot \ of \ log_2FoldChange \ in \ transcript \ plotted \ against \ -log10(\textit{P}_{adj} \ value) \ for \ dex \ begin{picture}(100,00) \put(0,0){\ otherwise} \put(0,0){$ (right, blue) against ctrl samples at 72 h (left, pink). The gray dashed line indicates  $P_{\text{adj}}$  value = 0.05. Significance testing using a moderated t test. F: GSEA analysis of enriched biological pathways in Dex compared with Ctrl at the 72 h time point. G: plot of genes belonging to the top three activated biological processes from F. Colors correspond to the  $\log_2$ FoldChanges in normalized counts of transcripts. Only genes with  $\log_2$ FC  $\geq 2.5$  are shown. RNA-Seq data collected from  $4 \times$  biological replicates. Dex, dexamethasone; GO, gene ontology; GSEA, gene set enrichment analysis; MB, myoblasts; MT, myotubes.

and GO:0030239; Fig. 2C), including enrichment of genes encoding several thick and thin filaments and Z-disk proteins (Fig. 2D). Conversely, transcripts related to regulation of mitosis (e.g., mitotic spindle elongation; GO:0000022,

spindle checkpoint signaling; GO:0031577, and regulation of chromosome separation; GO: 1905818) were downregulated in myotubes. This included Zwint, Zwilch, Birc5, Cenpe, and Cdc20 (Supplemental Table S1).



In the 24-h dex-treated sample, pairwise comparison with vehicle-treated controls revealed significant induction of GCresponsive genes such as Tsc22d3, a GC-induced leucine zipper, and Fkbp5, a modulator of GR activity (Supplemental Fig. S1F) (41, 42). Interestingly, we also observed increased levels of Cblb, which encodes a ubiquitin E3 ligase that targets insulin receptor substrate 1 (IRS-1) for degradation, promoting FOXO3mediated atrogene expression (43). Moreover, Dcun1d3, a NEDD8 E3 ligase and one of the five mammalian homologs of yeast DcnI (44), was also increased. Because NEDD8 is a regulator of Cullin-type ubiquitin ligase activity, and given the growing list of these complexes reported to be associated with skeletal muscle atrophy, the upregulation of this protein suggests a potential novel regulatory role in skeletal muscle atrophy. Despite the differential expression of  $\sim$ 4,800 genes at this time point, GSEA analysis did not reveal significant enrichment of specific biological pathways.

In contrast, the 72-h dex-treated samples showed a distinct transcriptomic response. We observed reduced expression of Wisp1 and Wls (Fig. 2E), suggesting downregulation of the Wnt signaling pathway (45, 46). We also observed a continued increase of Tsc22d3 and Fkbp5 expression, along with several others already observed at 24 h (Vav2 and Ppl) (Fig. 2*E*). In fact,  $\sim$ 540 genes were significantly upregulated and ~300 genes downregulated at both 24 and 72 h of dextreatment compared with their respective vehicle-treated controls (Supplemental Fig. S1G,  $P_{\rm adj}$  value < 0.05, -1 < $log_2$ FoldChange < 0.5). GSEA analysis for the 72 h time point revealed enrichment of pathways related to DNA replication and mitotic progression (Fig. 2F). This was due to increased transcription of several kinesin family members (Kif2c, Kif4, Kif11, Kif14, and Kif15) and genes previously downregulated during myotube fusion (*Birc5*, Cdc20, and Cenpe) (Fig. 2G).

## **Alternative Splicing Dynamics During Atrophy**

To investigate whether myogenic differentiation and dexinduced myotube atrophy affect alternative splicing, we analyzed differential alternative splicing (DAS) events using a threshold of transcripts per million (TPM)>1. Across conditions, we detected 38,741 isoforms, with most genes expressing more than two isoforms (Fig. 3A). Although GSEA did not yield enriched pathways at 24 h, DAS analysis revealed biologically meaningful isoform switching in 416 genes, many involving changes in protein domains or intracellular localization (Fig. 3, A and B). In contrast, only 247 genes underwent isoform switching during differentiation from myoblasts to myotubes (Fig. 3B). Gene enrichment analysis of these 416 genes revealed a strong association with translational and posttranslational protein modifications (Fig. 3C,  $P_{\rm adj}$  value  $\leq$  0.05), highlighting an additional regulatory layer to be active during early stages of myotube atrophy.

Next, we examined whether genes undergoing DAS were also identified as differentially expressed genes (DEGs) to assess the extent to which isoform abundance influences total gene expression. Our results indicated that  $\sim$ 3.5 % of DEGs also exhibited DAS within the first 24 h of dex-induced atrophy (Fig. 3D). Interestingly, this overlap dropped to <1% at 72 h, despite a rise in the number of DEGs overall (Fig. 3E). These findings suggest that isoform-specific transcriptional regulation is largely confined to the early phase of atrophy. This temporal specificity was further supported by a reduction in the total number of DAS events at 72 h, where only 53 genes exhibited isoform switches between vehicle- and dextreated samples, and 198 genes showed changes between 24 and 72 h dex, a number considerably less than that observed at 24 h (Fig. 3*B*).

All genes that underwent both DEG and DAS are provided in Supplemental Table S2. Noteworthy among them at the 24-h time point were Dcun1d3, Ubr2, and Ubr5, and at the 72-h time point, Mylk4 (Fig. 3F) (DEG  $P_{adj}$  values: Dcun1d3:  $1.99 \times 10^{-31}$ , Ubr2: 0.031, Ubr5: 0.00031, and *Mylk4*:  $6.05 \times 10^{-11}$ ). *Ubr2 and Ubr5*, both encoding ubiquitin E3 ligases, have been previously associated with muscle atrophy and hypertrophy, respectively (47, 48). Both genes were significantly upregulated following 24 h of dex-treatment. Interestingly, *Ubr5* displayed isoform changes only in noncoding transcripts, whereas coding transcripts remained unchanged. In contrast, Ubr2 exhibited alternative splicing of a second coding isoform (ENSMUST00000113335.4), resulting in a protein variant differing by 13 amino acids compared with the reference sequence (Uniprot ID Q6WKZ8-1 vs. -2). Despite transcriptional upregulation, UBR2 protein levels decreased, whereas UBR5 protein abundance slightly increased under atrophy (Supplemental Fig. S1H).

At 72 h, Mylk4, a kinase acting on myosin light chains, whose expression in skeletal muscle increases with dihydrotestosterone treatment and enables Ca<sup>2+</sup>-induced contraction with a cardiac and a skeletal muscle variant (49), showed a shift in isoform expression. The skeletal muscle-specific isoform (ENSMUST00000238977.3) increased, whereas the cardiac variant (ENSMUST00000057428.13) was downregulated, suggesting that C2C12 myotubes differentiated with FBS may predominantly express the cardiac Mylk4 isoform. A third isoform (ENSMUST00000230119.2), also classified as proteincoding, was expressed at a higher level in controls.

# Mitochondrial Translation and Oxidative Phosphorylation Are Upregulated in Dexamethasone-**Induced Atrophy**

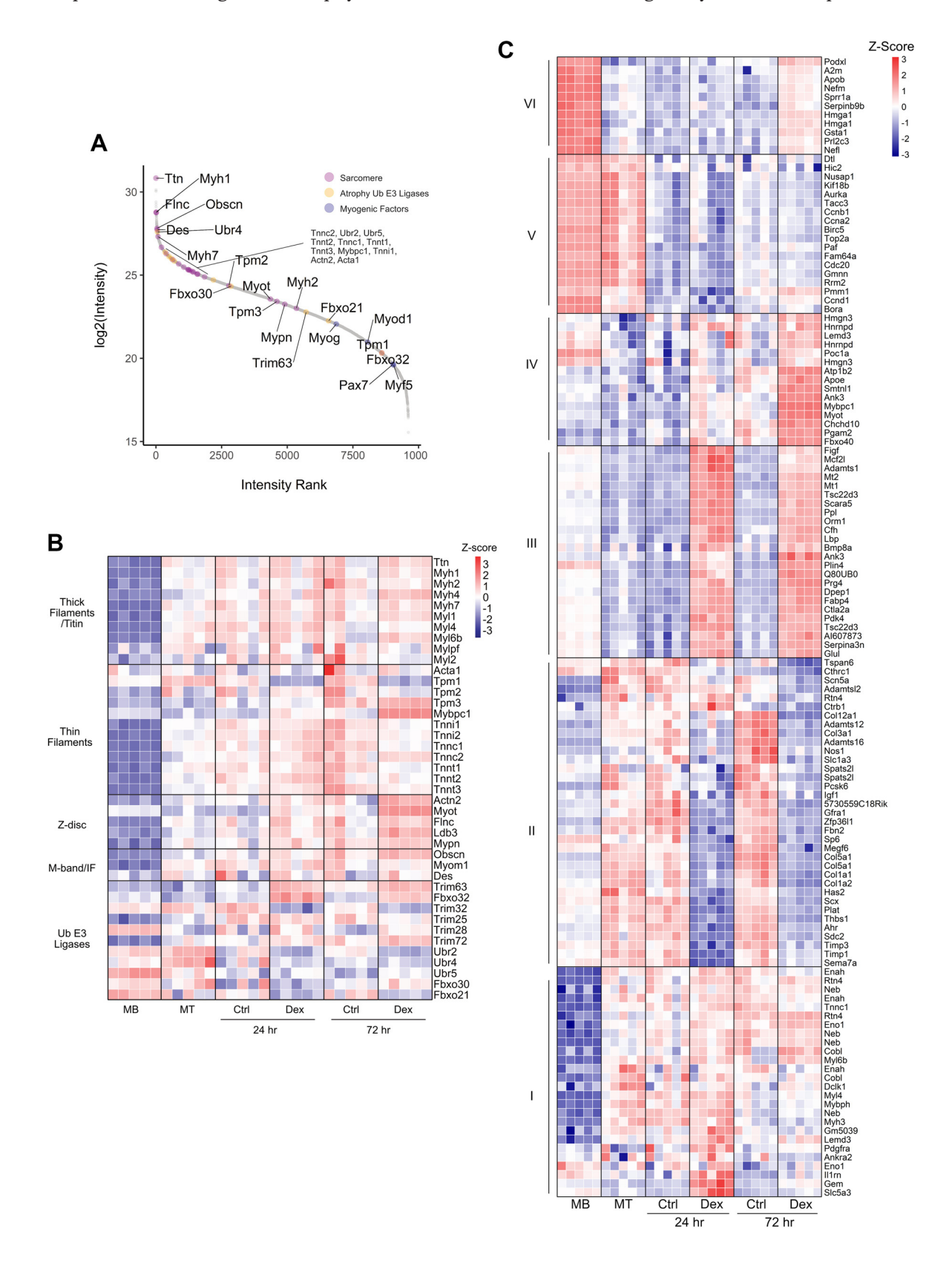
To study the proteomic landscape, we performed tandem mass tag mass spectrometry (TMT-MS) on proteins from C2C12 cells that were harvested at the same time points used

Figure 3. Differential alternative splicing (DAS) events in differentiation and dexamethasone atrophy in C2C12 cells. A: histogram of the number of isoforms per gene identified in the RNA-Seq experiment. TPM > 1. Counts >15 isoforms were negligible and are not included for legibility. B: number of DAS events identified per comparison ( $P_{\text{adj}} < 0.05$ ). Isoform switches were filtered for consequences (see IsoformSwitchAnalyzeR documentation). C: GSEA of enriched biological pathways from significant DAS genes between Dex and Ctrl 24 h using clusterProfiler. D: and E: Venn diagram of genes undergoing DAS and DEG for 24 h (D) and 72 h (E). This IsoformSwitchAnalyzeR analysis did not filter for biological consequences, since DEG does not take this into account. F: gene expression (top row) and isoform expression (bottom row) of Dcun1d3, Ubr2, and Ubr5 at 24 h or Mylk4 at 72 h post Dex or vehicle Ctrl treatment. Significance testing of gene expression by a moderated t test. n 4. Means  $\pm$  SD are plotted for each. DEG, differentially

expressed gene; Dex, dexamethasone; GSEA, gene set enrichment analysis; TPM, transcripts per million. \* $P \le 0.05$ , \*\* $P \le 0.01$ , \*\*\* $P \le 0.001$ .

for the RNA-Seq experiment. TMT-MS allows multiplexing of a large number of samples and is highly sensitive in detecting low-abundance proteins. This analysis enabled quantification of 9,613 proteins, including known atrophy markers such

as MuRF1/Trim63, MAFBx/Atrogin-1/Fbxo32, and MUSA1/ Fbxo30 (3, 4). This high coverage exceeds the typical 3,500-5,000 proteins quantified in mouse tissue, likely due to the homogeneity of cells compared with animal



tissue preparations, the presence of residual undifferentiated mononuclear cells (14, 16), or methodological differences. PCA showed good clustering of biological replicates for the individual samples, reflecting different stages of differentiation and atrophy (Supplemental Fig. S2A).

During differentiation, we observed increased expression of sarcomeric proteins (Fig. 4A), with MYH1 being the most abundant, followed by MYH7 and MYH4, suggesting a fiber type composition biased toward type IIx, type I, and type IIb fibers and low levels of type IIa (MYH2). Isoforms of troponin (C, I, and T) from both skeletal and cardiac muscle were also detected. MYH6, the second cardiac MyHC isoform, was absent or below the detection limit (Fig. 4A). Similarly, myosin light chain isoforms MYL3 and MYL7, representing ventricular and atrial cardiomyocyte forms, respectively (50), were not detected. In comparison with the highly abundant sarcomere components, which cluster in the higher intensity ranks, ubiquitin E3 ligases (including atrogenes) spanned a wide range of abundance, while myogenic regulators (MyoD1, myogenin, and PAX7) ranked lower, indicating minimal contamination from undifferentiated cells in myotube samples (Fig. 4A).

Contrary to our expectations, no general loss of sarcomeric proteins was observed with dex-treatment, with the exception of Ca<sup>2+</sup> sensing proteins, including Tropomyosin (TPM1 and TPM2) and Troponins (I, C, and T) (Fig. 4B). As anticipated, MuRF1 (Trim63) and Atrogin-1 (Fbxo32) increased along with Serpina3n, a recently proposed atrophy biomarker (Fig. 4, B and C; cluster III) (16, 51). However, other ubiquitin E3 ligases such as TRIM72, TRIM25, UBR4, UBR5, and FBXO30 showed minimal changes. Interestingly. TRIM32 and FBXO21/SMART were downregulated despite being linked to the degradation of desmin and Z-disks (5, 52) (Fig. 4B). Overall, this suggests that the C2C12 dex atrophy model recapitulates regulatory events from mouse tissue experiments but is less suited for studying sarcomere breakdown by TRIM32 or FBXO21/SMART. Additional UPS components with significant expression changes ( $P_{\text{adj}}$  value  $\leq$ 0.05) are detailed in Supplemental Fig. S2B.

Notably, the top 15 most regulated proteins during differentiation and atrophy did not include sarcomeric proteins or atrogenes (Fig. 4C). Both atrophy time points shared 485 upregulated proteins (cluster III), enriched in processes related to mitochondrial translation and mitochondrial gene expression (GO:0032543, GO:01450053) (Fig. 5, A and B). These included mitochondrial ribosomal proteins (MRPL1, MRPL3, MRPS22, and MRPS25) and respiratory chain components (COX5A, COX6C, and NDUFA9) (Fig. 5A, Supplemental Fig. S3). These changes were not paralleled at the mRNA level, suggesting translation from mRNA pools generated during differentiation (Supplemental Fig. S3). Remarkably, ERRα and NRF-1, two transcription factors promoting mitochondrial

gene expression, were significantly increased ( $P_{adi}$  value <0.0001, Supplemental Fig. S4A).

In contrast, cytoplasmic ribosomal subunits were substantially lower at both atrophy time points, likely contributing to the general decrease in protein translation observed in atrophic muscle (Supplemental Fig. S4, B and C) (53, 54). Additional downregulated proteins included those involved in skeletal muscle development and Wnt signaling (Fig. 5C), implicating an impairment of cell cycle progression during dex exposure. The collagen biosynthetic process was also downregulated, with several collagen proteins (Col1a1, Col1a2, Col5a1, Col3a1, and Col12a1) and tissue inhibitor of metalloprotease 1 (Timp1) decreasing with dex exposure (Fig. 4C; cluster II, Fig. 5C).

## mRNA and Protein Correlation Reveals **Posttranscriptional Control**

We next compared changes in RNA-Seq and proteomics data. The 24-h atrophy time point showed the strongest correlation between mRNA and protein changes ( $R^2 = 0.390$ ), followed by 72 h ( $R^2$  value = 0.340) (Fig. 6, A and B). However, the widespread of mRNA values (x-axis) relative to protein fold-changes (y-axis) at 72 h suggests impaired translation or posttranslational regulation. Surprisingly, differentiation (myoblast vs. myotube) had the lowest RNA-protein correlation ( $R^2$  value = 0.269, Supplemental Fig. S5), further supporting a delay or disconnect between transcription and translation during myogenic differentiation (16).

# **Prolonged Dexamethasone Exposure Better Mirrors In** Vivo Atrophy Profiles

To assess how closely our C2C12 model mimics in vivo responses, we compared our proteomic results with a mouse muscle TMT-MS dataset from 6-mo-old mice injected with 20 mg/kg/day of dexamethasone for 14 days (16). When pooling both atrophy time points, overlap with the mouse dataset was limited. However, separate comparisons showed that the 72 h C2C12 samples had greater concordance with the in vivo model (Fig. 7A) compared with the 24 h samples (Supplemental Fig. S6A).

We then performed GSEA to identify shared and unique biological processes. Common pathways enriched in both models included metabolic processes, such as that of monoatomic cation, α-amino acid, ROS, and lipid or fatty acids (GO:0055080, GO:1901605, GO:0072593, GO:0045834, and GO:0006631) (Fig. 7B). Downregulated pathways included actin cytoskeleton organization, vesicle-mediated transport, and cell migration properties (GO: 0030036, GO:0060627, and GO:0030335) (Fig. 7C). However, C2C12-specific enrichments included mitochondrial processes and ribosome biogenesis (GO:0032543, GO:0007005, and GO:0042254) (Supplemental

Figure 4. TMT-MS proteomic analyses of differentiation and dex-induced atrophy in C2C12 cells. A: intensity ranking of sarcomeric proteins (purple), ubiquitin (Ub) E3 ligases (yellow), and myogenic factors (blue). B: Z-score heat map of selected sarcomeric components and Ub E3 ligases associated with skeletal muscle atrophy. Genes were not filtered for significance. Each square corresponds to a biological replicate quantification. C: Z-score heat map of median-MAD normalized intensity values of top 15 genes with significant  $P_{\rm adj}$  value  $\leq$  0.05 from TMT-MS data. Up- or downregulation in comparisons of: MT vs. Dex 24 h, MT vs. Dex 72 h, Dex 24 h vs. Dex 72 h, Dex vs. Ctrl 24 h, Dex vs. Ctrl 72 h were pooled together and filtered for unique gene entries. Euclidean clustering was applied row-wise. HGNC gene names for proteins are indicated. Where there are duplicate gene names, the HGNC genes correspond to different Uniprot entries. Significance testing using a moderated t test. Data collected from 5x biological replicates. Dex, dexamethasone; MAD, median absolute deviation; MT, myotubes; TMT-MS, tandem mass tag mass spectrometry.

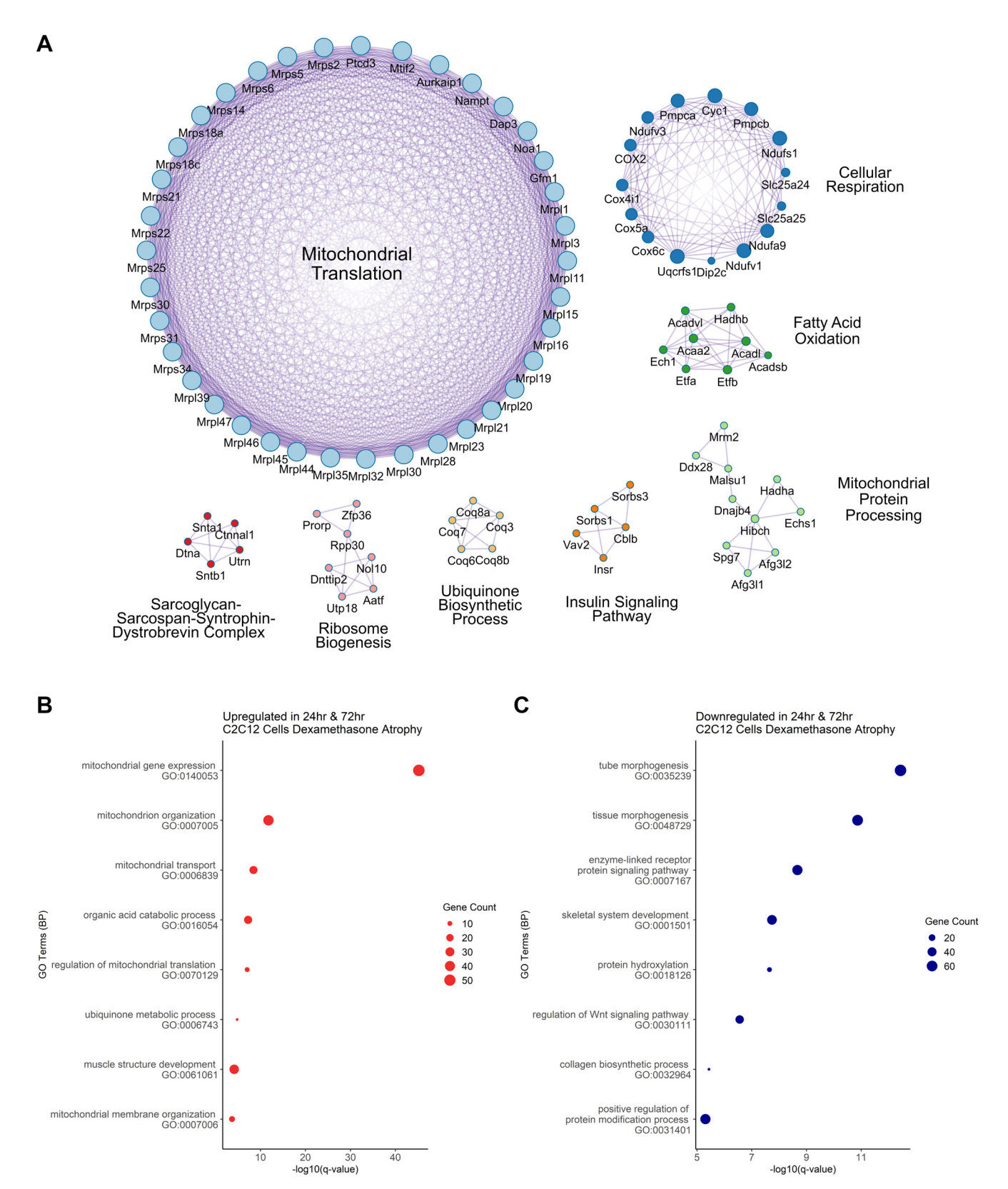


Figure 5. Protein-protein interaction enrichment analysis reveals significant enrichment of mitochondrial processes in dex-induced atrophy of C2C12 cells. A: protein-protein interaction enrichment analysis (Metascape) of upregulated proteins in both Dex 24 h and 72 h compared with respective Ctrl conditions, with  $P_{\text{adj}}$  value  $\leq 0.05$ . Figure created with Cytoscape. B and C: GO enrichment analysis of up- or downregulated proteins common to both 24 and 72 h dex atrophy in C2C12 cells with  $P_{adj}$  value  $\leq$  0.05 using STRING. Dex, dexamethasone; GO, gene ontology.

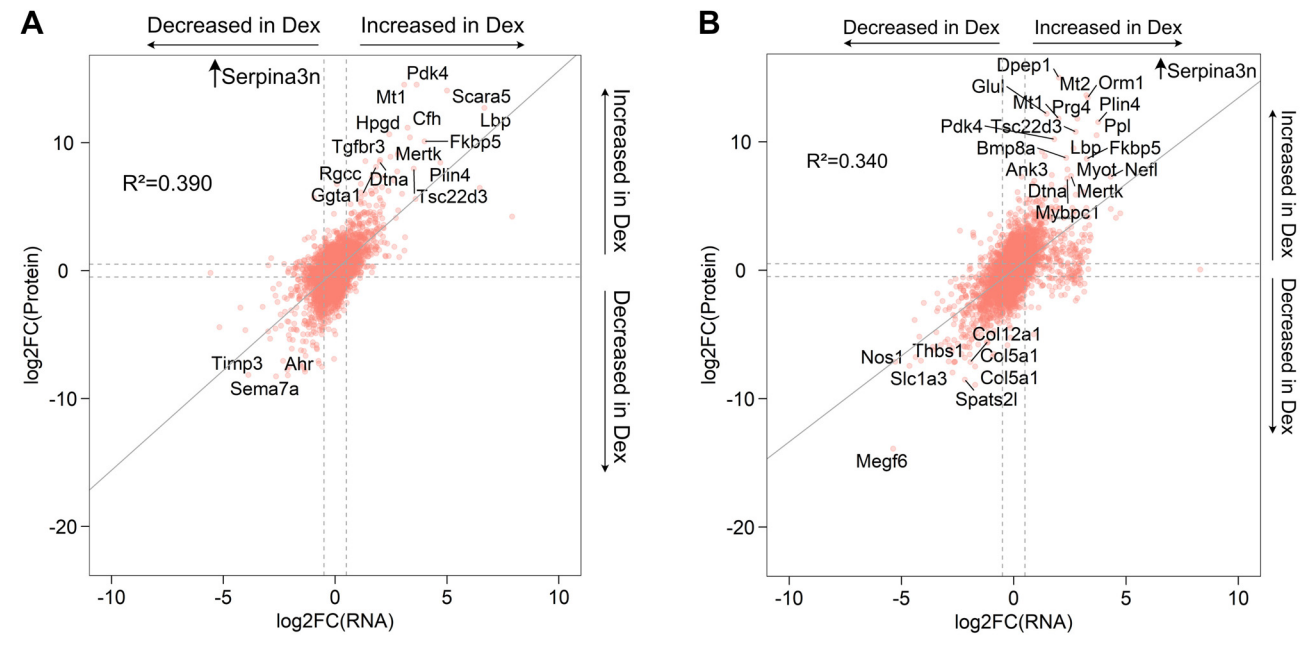


Figure 6. Integrated RNA-protein log\_foldchange of C2C12 cells under dex atrophy. A and B: log\_FoldChanges of RNA (x-axis) plotted against those of proteins identified by TMT-MS (y-axis) for Dex vs. Ctrl 24 h (A) and Dex vs. Ctrl 72 h (B). R<sup>2</sup> values were calculated based on linear regression modeling using R. Serpina3n (Serpina3n) has been omitted in both plots, due to the log<sub>2</sub>FC being significantly further from the rest of the data points. Where there are duplicate gene names, the HGNC genes correspond to different Uniprot entries. Dashed lines correspond to a 50% increase in abundance. Dex, dexamethasone; TMT-MS, tandem mass tag mass spectrometry.

Fig. S6B). Downregulation involved more processes related to the Golgi (Golgi vesicle transport, Golgi organization) and tube morphogenesis (Supplemental Fig. S6B). Interestingly, in mouse tissue, mitochondrial gene expression was suppressed, along with membrane organization and regulation of vesicle-mediated transport, whereas no specific skeletal muscle-related processes were activated (Supplemental Fig. S6C). This highlights a biological mismatch between in vitro and in vivo systems.

#### **DISCUSSION**

Endogenous glucocorticoid hormones play an essential role in maintaining protein homeostasis in skeletal muscle, balancing protein synthesis and degradation. Clinically, GCs are commonly used to dampen inflammation via its inhibitory effects on the NF-κB pathway (8, 55). However, chronic or high-dose GC exposure is known to induce muscle atrophy through transcriptional regulation via the GR, which leads to muscle protein degradation (9). Although animal models have provided important insights into GC-induced muscle atrophy, cell culture model systems offer a scalable and controllable method to study these mechanisms in better resolution. Here, we present a comprehensive multiomics dataset profiling transcriptomic, proteomic, and splicing dynamics in C2C12 myotubes undergoing dexinduced atrophy.

The C2C12 cell line is a widely used model for studying skeletal muscle development and atrophy. Our data indicate that extending differentiation to day 7, beyond the commonly used 3-5 day window, more faithfully replicates the mature sarcomere environment and better models in vivo atrophy responses. This was apparent based on the increased

fusion index, myotube diameters, and enrichment of structural and contractile component characteristics for mature muscle. Since the C2C12 cell line cannot be reproducibly cultured past day 10 without loss of adherence or cultured past passage 12–15 without loss of differentiation properties, this defines a practical experimental window for modeling atrophy in vitro.

We observed a high degree of overlap between data from mouse tissue in mRNA and protein patterns during the transition of undifferentiated myoblasts to differentiated myotubes. This included enrichment of Z-disk components and thick and thin filaments, along with an increase of myogenic factors such as Myomaker, Myomixer, Myogenin, and MYF5. These observations are further supported by measurements of cell morphology. Together, our results suggest that the mRNA and proteomic data from C2C12 cells provide robust information about fusion and differentiation hallmarks of muscle cells and will thereby aid further studies of sarcomere formation.

Upon dex treatment, we detected an increase of mRNAs and proteins associated with mitochondrial protein expression, whereas mRNAs for factors involved in DNA replication and mitosis were reduced. This seemingly contradicts previous findings from mouse tissue that implicated mitochondrial dysfunction as a hallmark of atrophy (16, 56). This could be explained by differences in the duration of dextreatment (14 days in mice vs. 3 days in C2C12 cells) or dosage, especially given that lower dex administration in 4-day differentiated C2C12 myotubes showed compromised oxidative capacity (57). Our dataset also does not show downregulation of sarcomeric proteins despite expression of atrogenes (MuRF1, MAFbx/Atrogin-1, and TRIM72) and GC-responsive protein expression (TSC22D3 and FKBP5). On the contrary,



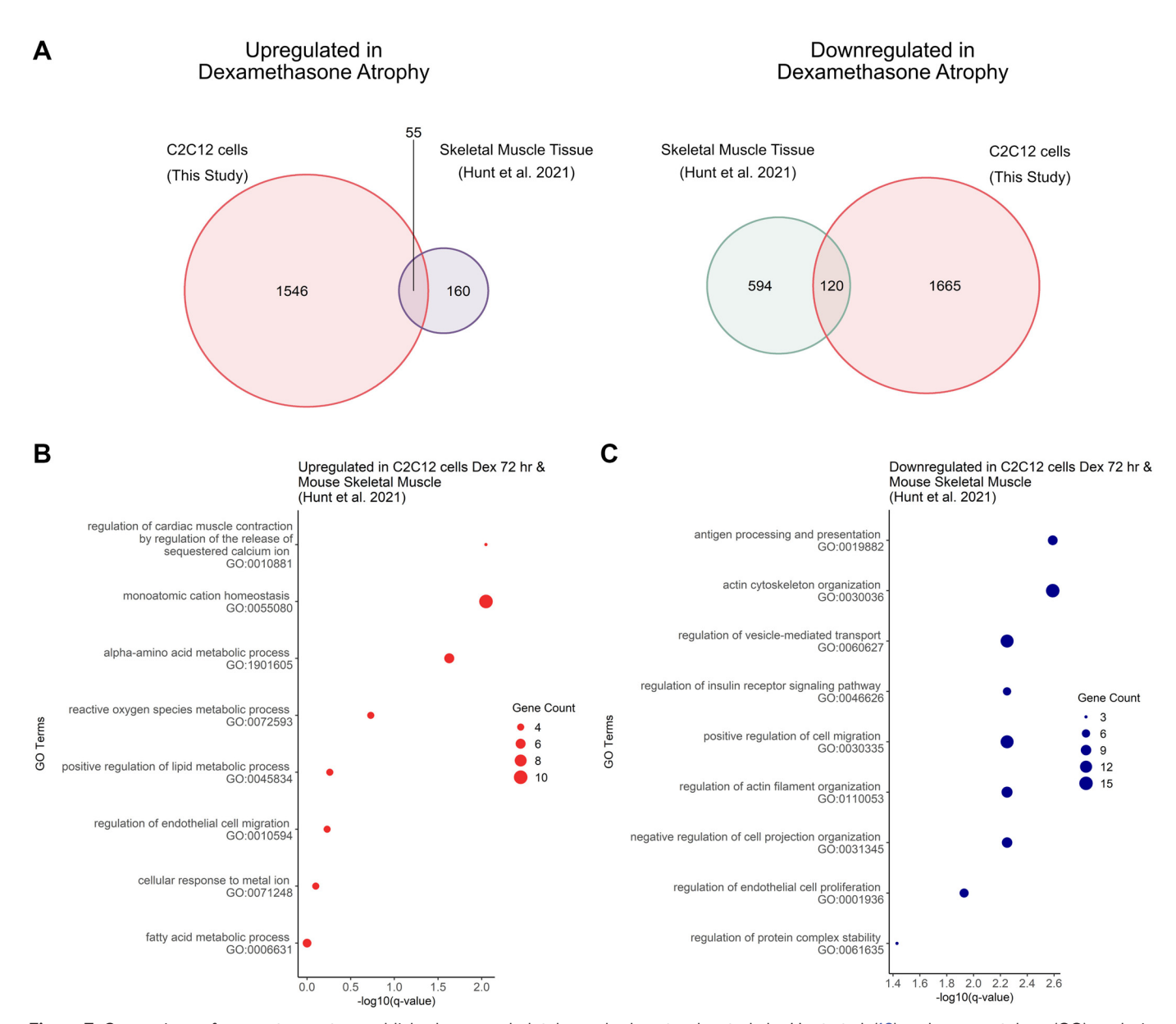


Figure 7. Comparison of our proteome to a published mouse skeletal muscle dex atrophy study by Hunt et al. (16) and gene ontology (GO) analysis. A: overlap of proteins significantly changing in Dex vs. Ctrl 72 h in this study (n = 5) compared with mouse skeletal muscle dex atrophy data from the study by Hunt et al. (16), where mice were treated for 14 days with 20 mg/kg/day dex ( $n = P_{adj}$  value  $\le 0.05$  in both,  $-1 \le \log_2 FC \le 0.6$  applied for C2C12 TMT-MS dataset,  $-0.3 < \log_2 FC < 0.3$  applied for Hunt et al. (16) TMT-MS data). B: GO analysis of 54 proteins increased in this study and Hunt et al. (16) dataset in the left Venn diagram from A using STRING. C: GO analysis of 44 proteins decreased in this study and Hunt et al. (16) dataset in the right Venn diagram from A using STRING. Dex, dexamethasone; TMT-MS, tandem mass tag mass spectrometry.

we also saw a significant decrease in cytosolic ribosome expression, which is in line with an impaired overall protein synthesis that has previously been observed in other atrophy models (54). Presumably, our dataset captures earlier events leading up to sarcomeric protein degradation, when myotubes still retain sarcomeric proteins, albeit either posttranslationally modified or disassembled. Evidence of phosphorylation and ubiquitination preceding disassembly and subsequent degradation has been reported for the intermediate filament protein desmin (58). In our transcriptomic and proteomic data, collagen as well as TIMP1 expression decreased, which hints at increased metalloproteinase activity for extracellular matrix turnover and

therefore potential steps toward sarcomeric disassembly (59). Other studies also support that C2C12s may replicate "early" atrophy responses as defined in mice: a biphasic expression pattern has been reported for proteasomal subunits (RPN9, Gankyrin) and MuRF1 under denervation atrophy (60) with similar transcriptional changes in cancer cachexia (61). Comparison of a mouse dex atrophy model (16) indeed points toward this hypothesis, as we saw greater overlap with our 72 h time point data.

Although in this study, we defined 24 h as "early" and 72 h as "late" relative to C2C12 culture times, we still found clear differences in transcriptomic and proteomic signatures relative to controls. This suggests a dynamic response to atrophy stimuli already in what one may consider the "early phase" in animal studies. Whether the degradation of sarcomeric components can then be captured from a day 5 myotube state to maximize atrophy treatment time and better align in vivo models would be of interest in future studies. This may also provide insight into transcription/translation cyclical rhythms, explaining the biphasic atrophy response observed by others (60, 61).

Beyond differential expression, our transcriptomic analysis revealed widespread differential alternative splicing (DAS) at the early phase of atrophy, with fewer events at 72 h. Here, we observed a strong shift in isoform landscape without significant gene set enrichment in the GSEA analysis at 24 h. Although we have not performed RNA-binding protein motif enrichment or functional validation, these isoform switches, especially in genes such as *Dcun1d3*, Ubr2, Ubr5, and Mylk4, may alter protein interactions, localization, and function. For example, the observed isoformspecific shift in *Ubr2* (leading to a 13-amino acid variation) and the reduction in UBR2 protein despite increased transcript levels point to complex posttranscriptional or translational regulation. Such transcription and translation mismatch with a layer of splicing regulation could contribute to the resulting stimulus-specific atrophy phenotypes. The rest of the abovementioned proteins have previously been associated with cachexia or protein anabolism, with the exception of DCUN1D3 (47, 48, 62). Given the published involvement of Cullin complexes in atrophy, we hypothesize that NEDD8 E3 ligases are involved in this phenotype (3, 33, 63).

A meta-analysis of array-based transcriptomic data from mice, rat, and human tissues with corresponding cell lines revealed the same species to have the best correlation (18). More importantly, C2C12 performed most comparable with human primary cells in terms of its transcriptional profile for skeletal muscle function and contraction (18). Our data show that dex-treated C2C12 myotubes apparently represent early stages of muscle atrophy well while replicating later atrophy phenotypes poorly. We also identified new proteins to be possibly involved in atrophy, such as DCUN1D3, and shed light on alternative splicing events potentially worth further investigation. Thus, processes like recovery from sarcomere damage and proof of principle studies for atrophy prevention still ultimately rely on the analysis of muscle tissues—vet, for the identification of early indicators for chronic muscle wasting and initial design of therapeutic compounds to counteract muscle wasting onset, the C2C12 cell line still has much to offer. It is therefore a worthwhile alternative to consider and incorporate to reduce animal experimentation, save on time and financial resources, and provide a more ethically responsible approach to skeletal muscle research.

#### **DATA AVAILABILITY**

The original contributions presented in the study are included in the article and supplementary material. RNA-Seq data were deposited into the Gene Expression Omnibus database under Accession No. GSE300503 and can be accessed from the following URL: https://www.ncbi.nlm.nih.gov/geo/guery/acc.cgi? acc=GSE300503. The mass spectrometry proteomics data have

been deposited to the ProteomeXchange Consortium (http:// proteomecentral.proteomexchange.org) via the PRIDE partner repository (64) with the dataset identifier PXD064871.

#### SUPPLEMENTAL MATERIAL

Supplemental Fig. S1-S6 and Supplemental Tables S1 and S2: https://doi.org/10.6084/m9.figshare.29940209.v1.

## ACKNOWLEDGMENTS

The authors thank Corinna Volkwein and Mandy Gerlach for excellent technical help and Benjamin Sünkel for scientific discussion. We also thank the Advanced Light Microscopy facility (MDC) for assistance in confocal imaging; Dr. Tatiana Borodina and Dr. Daniele Yumi Sunaga-Franze at the genomics sequencing facility (MDC) for assistance in RNA-Seq and data preprocessing; Prof. Dr. Uta Höpken (MDC) for access to the BioAnalyzer; and Dr. Cristina Brischetto (TU-Berlin) for advice on RT-qPCR experiments. We also thank Dr. Dermot Harnett and Prof. Dr. Uwe Ohler (MDC) for data analysis assistance.

Preprint is available at https://doi.org/10.1101/2025.06.12.659253.

#### GRANTS

S.N. was a recipient of the International PhD fellowship from the Max Delbrück Center for Molecular Medicine in the Helmholtz Association. This study was supported by the Deutsche Forschungsgemeinschaft (DFG) Grants SO 271/10-1 (to T.S.) and FI965/10-1 (to J.F.) and the German Center for Cardiovascular Research, partner site Greifswald, Grant DZHK 81Z5400153 (to J.F.).

#### DISCLOSURES

No conflicts of interest, financial or otherwise, are declared by the authors.

#### AUTHOR CONTRIBUTIONS

S.N., P.M., E.J., J.F., and T.S. conceived and designed research; S.N. and O.P. performed experiments: S.N., A.M., and O.P. analyzed data; S.N. interpreted results of experiments; S.N. and A.M. prepared figures; S.N. drafted manuscript; S.N., P.M., E.J., J.F., and T.S. edited and revised manuscript; S.N., A.M., O.P., P.M., E.J., J.F., and T.S. approved final version of manuscript.

# REFERENCES

- Wing SS, Goldberg AL. Glucocorticoids activate the ATP-ubiquitindependent proteolytic system in skeletal muscle during fasting. Am J Physiol Endocrinol Physiol 264: E668-E676, 1993. doi:10.1152/ ajpendo.1993.264.4.E668.
- Schiaffino S, Dyar KA, Ciciliot S, Blaauw B, Sandri M. Mechanisms regulating skeletal muscle growth and atrophy. FEBS J 280: 4294-4314, 2013. doi:10.1111/febs.12253.
- Bodine SC, Latres E, Baumhueter S, Lai VK, Nunez L, Clarke BA, Poueymirou WT, Panaro FJ, Na E, Dharmarajan K, Pan ZQ, Valenzuela DM, DeChiara TM, Stitt TN, Yancopoulos GD, Glass DJ. Identification of ubiquitin ligases required for skeletal muscle atrophy. Science 294: 1704-1708, 2001. doi:10.1126/science.1065874.
- Sartori R, Schirwis E, Blaauw B, Bortolanza S, Zhao J, Enzo E, Stantzou A, Mouisel E, Toniolo L, Ferry A, Stricker S, Goldberg AL, Dupont S, Piccolo S, Amthor H, Sandri M. BMP signaling controls muscle mass. Nat Genet 45: 1309–1318, 2013. doi:10.1038/ng.2772.
- Milan G, Romanello V, Pescatore F, Armani A, Paik J-H, Frasson L, Seydel A, Zhao J, Abraham R, Goldberg AL, Blaauw B, DePinho RA, Sandri M. Regulation of autophagy and the ubiquitin-

- proteasome system by the FoxO transcriptional network during muscle atrophy. Nat Commun 6: 6670, 2015. doi:10.1038/ ncomms7670.
- Sandri M, Sandri C, Gilbert A, Skurk C, Calabria E, Picard A, Walsh K, Schiaffino S, Lecker SH, Goldberg AL. Foxo transcription factors induce the atrophy-related ubiquitin ligase atrogin-1 and cause skeletal muscle atrophy. Cell 117: 399-412, 2004. doi:10.1016/s0092-8674(04)00400-3.
- Waddell DS, Baehr LM, van den Brandt J, Johnsen SA, Reichardt HM, Furlow JD, Bodine SC. The glucocorticoid receptor and FOXO1 synergistically activate the skeletal muscle atrophy-associated MuRF1 gene. Am J Physiol Endocrinol Physiol E785-E797, 2008. doi:10.1152/ajpendo.00646.2007.
- Auphan N, DiDonato JA, Rosette C, Helmberg A, Karin M. Immunosuppression by glucocorticoids: inhibition of NF-kappa B activity through induction of I kappa B synthesis. Science 270: 286-290, 1995. doi:10.1126/science.270.5234.286.
- Shimizu N, Yoshikawa N, Ito N, Maruyama T, Suzuki Y, Takeda SI, Nakae J, Tagata Y, Nishitani S, Takehana K, Sano M, Fukuda K, Suematsu M, Morimoto C, Tanaka H. Crosstalk between glucocorticoid receptor and nutritional sensor mTOR in skeletal muscle. Cell Metab 13: 170-182, 2011. doi:10.1016/j.cmet.2011.01.001.
- Lecker SH, Solomon V, Mitch WE, Goldberg AL. Muscle protein breakdown and the critical role of the ubiquitin-proteasome pathway in normal and disease states. J Nutr 129: 227S-237S, 1999. doi:10. 1093/jn/129.1.227S.
- McDonald CM, Henricson EK, Abresch RT, Duong T, Joyce NC, Hu F, Clemens PR, Hoffman EP, Cnaan A, Gordish-Dressman H; CINRG Investigators. Long-term effects of glucocorticoids on function, quality of life, and survival in patients with Duchenne muscular dystrophy: a prospective cohort study. Lancet 391: 451–461, 2018. doi:10.1016/S0140-6736(17)32160-8.
- Baltgalvis KA, Call JA, Nikas JB, Lowe DA. Effects of prednisolone on skeletal muscle contractility in mdx mice. Muscle Nerve 40: 443-454, 2009. doi:10.1002/mus.21327.
- Lang F, Aravamudhan S, Nolte H, Türk C, Hölper S, Müller S, Günther S, Blaauw B, Braun T, Krüger M. Dynamic changes in the skeletal muscle proteome during denervation-induced atrophy. Dis Model Mech 10: 881-896, 2017. doi:10.1242/dmm.028910.
- Lang F, Khaghani S, Türk C, Wiederstein JL, Hölper S, Piller T, Nogara L, Blaauw B, Günther S, Müller S, Braun T, Krüger M. Single muscle fiber proteomics reveals distinct protein changes in slow and fast fibers during muscle atrophy. J Proteome Res 17: 3333-3347, 2018. doi:10.1021/acs.jproteome.8b00093.
- Shavlakadze T, Morris M, Fang J, Wang SX, Zhu J, Zhou W, Tse HW, Mondragon-Gonzalez R, Roma G, Glass DJ. Age-related gene expression signature in rats demonstrate early, late, and linear transcriptional changes from multiple tissues. Cell Rep 28: 3263-3273.e3, 2019. doi:10.1016/j.celrep.2019.08.043.
- Hunt LC, Graca FA, Pagala V, Wang YD, Li Y, Yuan ZF, Fan Y, Labelle M, Peng J, Demontis F. Integrated genomic and proteomic analyses identify stimulus-dependent molecular changes associated with distinct modes of skeletal muscle atrophy. Cell Rep 37: 109971, 2021. doi:10.1016/j.celrep.2021.109971.
- Hitachi K, Nakatani M, Kiyofuji Y, Inagaki H, Kurahashi H, Tsuchida K. An analysis of differentially expressed coding and long non-coding RNAs in multiple models of skeletal muscle atrophy. Int J Mol Sci 22: 2558, 2021. doi:10.3390/ijms22052558.
- Abdelmoez AM, Sardón Puig L, Smith JAB, Gabriel BM, Savikj M, Dollet L, Chibalin AV, Krook A, Zierath JR, Pillon NJ. Comparative profiling of skeletal muscle models reveals heterogeneity of transcriptome and metabolism. Am J Physiol Cell Physiol 318: C615-C626, 2020. doi:10.1152/ajpcell.00540.2019.
- Hughes DC, Goodman CA, Baehr LM, Gregorevic P, Bodine SC. A critical discussion on the relationship between E3 ubiquitin ligases, protein degradation, and skeletal muscle wasting: it's not that simple. Am J Physiol Cell Physiol 325: C1567-C1582, 2023. doi:10.1152/ ajpcell.00457.2023.
- Mertins P, Tang LC, Krug K, Clark DJ, Gritsenko MA, Chen L, Clauser KR, Clauss TR, Shah P, Gillette MA, Petyuk VA, Thomas SN, Mani DR, Mundt F, Moore RJ, Hu Y, Zhao R, Schnaubelt M, Keshishian H, Monroe ME, Zhang Z, Udeshi ND, Mani D, Davies SR, Townsend RR, Chan DW, Smith RD, Zhang H, Liu T, Carr SA. Reproducible workflow for multiplexed deep-scale proteome and

- phosphoproteome analysis of tumor tissues by liquid chromatography-mass spectrometry. Nat Protoc 13: 1632-1661, 2018. doi:10. 1038/s41596-018-0006-9.
- Ritchie ME, Phipson B, Wu D, Hu Y, Law CW, Shi W, Smyth GK. limma powers differential expression analyses for RNA-sequencing and microarray studies. Nucleic Acids Res 43: e47, 2015. doi:10. 1093/nar/gkv007.
- Wu T, Hu E, Xu S, Chen M, Guo P, Dai Z, Feng T, Zhou L, Tang W, Zhan L, Fu X, Liu S, Bo X, Yu G. clusterProfiler 4.0: a universal enrichment tool for interpreting omics data. Innovation (Camb) 2: 100141, 2021. doi:10.1016/j.xinn.2021.100141.
- Yu G, Wang LG, Yan GR, He QY. DOSE: an R/Bioconductor package for disease ontology semantic and enrichment analysis. *Bioinformatics* 31: 608-609. 2015. doi:10.1093/bioinformatics/btu684.
- Zhou Y, Zhou B, Pache L, Chang M, Khodabakhshi AH, Tanaseichuk O, Benner C, Chanda SK. Metascape provides a biologist-oriented resource for the analysis of systems-level datasets. Nat Commun 10: 1523, 2019. doi:10.1038/s41467-019-09234-6.
- Shannon P, Markiel A, Ozier O, Baliga NS, Wang JT, Ramage D, Amin N, Schwikowski B, Ideker T. Cytoscape: a software environment for integrated models of biomolecular interaction networks. Genome Res 13: 2498-2504, 2003. doi:10.1101/gr.1239303.
- Schindelin J, Arganda-Carreras I, Frise E, Kaynig V, Longair M, Pietzsch T, Preibisch S, Rueden C, Saalfeld S, Schmid B, Tinevez JY, White DJ, Hartenstein V, Eliceiri K, Tomancak P, Cardona A. Fiji: an open-source platform for biological-image analysis. Nat Methods 9: 676-682, 2012. doi:10.1038/nmeth.2019.
- Braun TP, Zhu X, Szumowski M, Scott GD, Grossberg AJ, Levasseur PR, Graham K, Khan S, Damaraju S, Colmers WF, Baracos VE, Marks DL. Central nervous system inflammation induces muscle atrophy via activation of the hypothalamic-pituitary-adrenal axis. J Exp Med 208: 2449–2463, 2011. doi:10.1084/jem.20111020.
- Cooper ST, Maxwell AL, Kizana E, Ghoddusi M, Hardeman EC, Alexander IE, Allen DG, North KN. C2C12 Co-culture on a fibroblast substratum enables sustained survival of contractile, highly differentiated myotubes with peripheral nuclei and adult fast myosin expression. Cell Motil Cytoskeleton 58: 200-211, 2004. doi:10.1002/cm. 20010.
- Ferri P. Barbieri E. Burattini S. Guescini M. D'Emilio A. Biagiotti L. Del Grande P, De Luca A, Stocchi V, Falcieri E. Expression and subcellular localization of myogenic regulatory factors during the differentiation of skeletal muscle C2C12 myoblasts. J Cell Biochem 108: 1302-1317, 2009. doi:10.1002/jcb.22360.
- Smith CW, Klaasmeyer JG, Edeal JB, Woods TL, Jones SJ. Effects of serum deprivation, insulin and dexamethasone on polysome percentages in C2C12 myoblasts and differentiating myoblasts. Tissue Cell 31: 451-458, 1999. doi:10.1054/tice.1999.0053
- Clarke BA, Drujan D, Willis MS, Murphy LO, Corpina RA, Burova E, Rakhilin SV, Stitt TN, Patterson C, Latres E, Glass DJ. The E3 ligase MuRF1 degrades myosin heavy chain protein in dexamethasonetreated skeletal muscle. Cell Metab 6: 376-385, 2007. doi:10.1016/j. cmet.2007.09.009.
- Nishimura M, Nikawa T, Kawano Y, Nakayama M, Ikeda M. Effects of dimethyl sulfoxide and dexamethasone on mRNA expression of housekeeping genes in cultures of C2C12 myotubes. Biochem Biophys Res Commun 367: 603-608, 2008. doi:10.1016/j.bbrc.2008. 01.006
- Nowak M, Suenkel B, Porras P, Migotti R, Schmidt F, Kny M, Zhu X, Wanker EE, Dittmar G, Fielitz J, Sommer T. DCAF8, a novel MuRF1 interaction partner, promotes muscle atrophy. J Cell Sci 132: jcs233395, 2019. doi:10.1242/jcs.233395.
- Rudnicki MA, Schnegelsberg PNJ, Stead RH, Braun T, Arnold HH, Jaenisch R. MyoD or Myf-5 is required for the formation of skeletal muscle. Cell 75: 1351-1359, 1993. doi:10.1016/0092-8674(93)90621-v.
- Wright WE, Sassoon DA, Lin VK. Myogenin, a factor regulating myogenesis, has a domain homologous to MyoD. Cell 56: 607-617, 1989. doi:10.1016/0092-8674(89)90583-7.
- Millay DP, O'Rourke JR, Sutherland LB, Bezprozvannaya S, Shelton JM, Bassel-Duby R, Olson EN. Myomaker is a membrane activator of myoblast fusion and muscle formation. Nature 499: 301-305, 2013. doi:10.1038/nature12343.
- Bi P, Ramirez-Martinez A, Li H, Cannavino J, McAnally JR, Shelton JM, Sánchez-Ortiz E, Bassel-Duby R, Olson EN. Control of muscle

- formation by the fusogenic micropeptide myomixer. Science 356: 323-327, 2017. doi:10.1126/science.aam9361.
- Price MG, Landsverk ML, Barral JM, Epstein HF. Two mammalian UNC-45 isoforms are related to distinct cytoskeletal and musclespecific functions. J Cell Sci 115: 4013-4023, 2002. doi:10.1242/jcs.
- 39. Lee CS, Yi JS, Jung SY, Kim BW, Lee NR, Choo HJ, Jang SY, Han J, Chi SG, Park M, Lee JH, Ko YG. TRIM72 negatively regulates myogenesis via targeting insulin receptor substrate-1. Cell Death Differ 17: 1254-1265, 2010. doi:10.1038/cdd.2010.1.
- Chin ER. Role of Ca<sup>2+</sup>/calmodulin-dependent kinases in skeletal muscle plasticity. J Appl Physiol (1985) 99: 414-423, 2005. doi:10. 1152/japplphysiol.00015.2005.
- D'Adamio F, Zollo O, Moraca R, Ayroldi E, Bruscoli S, Bartoli A, Cannarile L, Migliorati G, Riccardi C. A new dexamethasoneinduced gene of the leucine zipper family protects T lymphocytes from TCR/CD3-activated cell death. Immunity 7: 803-812, 1997. doi:10.1016/s1074-7613(00)80398-2.
- Wochnik GM, Rüegg J, Abel GA, Schmidt U, Holsboer F, Rein T. FK506-binding proteins 51 and 52 differentially regulate dynein interaction and nuclear translocation of the glucocorticoid receptor in mammalian cells. J Biol Chem 280: 4609-4616, 2005. doi:10. 1074/jbc.M407498200.
- Nakao R, Hirasaka K, Goto J, Ishidoh K, Yamada C, Ohno A, Okumura Y, Nonaka I, Yasutomo K, Baldwin KM, Kominami E, Higashibata A, Nagano K, Tanaka K, Yasui N, Mills EM, Takeda S, Nikawa T. Ubiquitin ligase Cbl-b is a negative regulator for insulinlike growth factor 1 signaling during muscle atrophy caused by unloading. Mol Cell Biol 29: 4798-4811, 2009. doi:10.1128/MCB. 01347-08.
- 44. Keuss MJ, Thomas Y, Mcarthur R, Wood NT, Knebel A, Kurz T. Characterization of the mammalian family of DCN-type NEDD8 E3 ligases. J Cell Sci 129: 1441-1454, 2016. doi:10.1242/jcs.181784.
- Cadigan KM. Wnt-β-catenin signaling. Current Biology 18: R943-R947, 2008. doi:10.1016/j.cub.2008.08.017.
- Jung TW, Kang C, Goh J, Chae SI, Kim HC, Lee TJ, Abd El-Aty AM, Jeong JH. WISP1 promotes non-alcoholic fatty liver disease and skeletal muscle insulin resistance via TLR4/JNK signaling. J Cell Physiol 233: 6077-6087, 2018. doi:10.1002/jcp.26449.
- Gao S, Zhang G, Zhang Z, Zhu JZ, Li L, Zhou Y, Rodney GG, Abo-Zahrah RS, Anderson L, Garcia JM, Kwon YT, Li YP. UBR2 targets myosin heavy chain IIb and IIx for degradation: molecular mechanism essential for cancer-induced muscle wasting. Proc Natl Acad Sci USA 119: e2200215119, 2022. doi:10.1073/pnas.2200215119.
- Hughes DC, Turner DC, Baehr LM, Seaborne RA, Viggars M, Jarvis JC, Gorski PP, Stewart CE, Owens DJ, Bodine SC, Sharples AP. Knockdown of the E3 ubiquitin ligase UBR5 and its role in skeletal muscle anabolism. Am J Physiol Cell Physiol 320: C45-C56, 2021. doi:10.1152/ajpcell.00432.2020.
- Sakakibara I, Yanagihara Y, Himori K, Yamada T, Sakai H, Sawada Y, Takahashi H, Saeki N, Hirakawa H, Yokoyama A, Fukada SI, Sawasaki T, Imai Y. Myofiber androgen receptor increases muscle strength mediated by a skeletal muscle splicing variant of Mylk4. iScience 24: 102303, 2021 [Erratum in iScience 28: 112643, 2025]. doi:10.1016/j.isci.2021.102303.
- Schiaffino S, Reggiani C. Fiber types in mammalian skeletal muscles. Physiol Rev 91: 1447-1531, 2011. doi:10.1152/physrev.00031. 2010.

- Gueugneau M, d'Hose D, Barbé C, de Barsy M, Lause P, Maiter D, Bindels LB, Delzenne NM, Schaeffer L, Gangloff YG, Chambon C, Coudy-Gandilhon C, Béchet D, Thissen JP. Increased Serpina3n release into circulation during glucocorticoid-mediated muscle atrophy. J Cachexia Sarcopenia Muscle 9: 929-946, 2018. doi:10.1002/ jcsm.12315.
- Cohen S, Zhai B, Gygi SP, Goldberg AL. Ubiquitylation by Trim32 causes coupled loss of desmin, Z-bands, and thin filaments in muscle atrophy. J Cell Biol 198: 575-589, 2012. doi:10.1083/jcb. 201110067
- Savary I, Debras E, Dardevet D, Sornet C, Capitan P, Prugnaud J, Mirand PP, Grizard J. Effect of glucocorticoid excess on skeletal muscle and heart protein synthesis in adult and old rats. Br J Nutr 79: 297-304, 1998. doi:10.1079/bjn19980047.
- Gordon BS, Kelleher AR, Kimball SR. Regulation of muscle protein synthesis and the effects of catabolic states. Int J Biochem Cell Biol 45: 2147–2157, 2013. doi:10.1016/j.biocel.2013.05.039.
- Schakman O, Kalista S, Barbé C, Loumaye A, Thissen JP. Glucocorticoid-induced skeletal muscle atrophy. Int J Biochem Cell Biol 45: 2163-2172, 2013. doi:10.1016/j.biocel.2013.05.036.
- Brown JL, Rosa-Caldwell ME, Lee DE, Blackwell TA, Brown LA, Perry RA, Haynie WS, Hardee JP, Carson JA, Wiggs MP, Washington TA, Greene NP. Mitochondrial degeneration precedes the development of muscle atrophy in progression of cancer cachexia in tumour-bearing mice. J Cachexia Sarcopenia Muscle 8: 926-938, 2017. doi:10.1002/jcsm.12232.
- Liu J, Peng Y, Wang X, Fan Y, Qin C, Shi L, Tang Y, Cao K, Li H, Long J, Liu J. Mitochondrial dysfunction launches dexamethasoneinduced skeletal muscle atrophy via AMPK/FOXO3 signaling. Mol Pharm 13: 73–84, 2016. doi:10.1021/acs.molpharmaceut.5b00516.
- Volodin A, Kosti I, Goldberg AL, Cohen S. Myofibril breakdown during atrophy is a delayed response requiring the transcription factor PAX4 and desmin depolymerization. Proc Natl Acad Sci USA 114: E1375-E1384, 2017. doi:10.1073/pnas.1612988114.
- Visse R, Nagase H. Matrix metalloproteinases and tissue inhibitors of metalloproteinases: structure, function, and biochemistry. Circ Res 92: 827-839, 2003. doi:10.1161/01.RES.0000070112.80711.3D.
- Gilda JE, Nahar A, Kasiviswanathan D, Tropp N, Gilinski T, Lahav T, Alexandrovich D, Mandel-Gutfreund Y, Park S, Shemer S. Proteasome gene expression is controlled by coordinated functions of multiple transcription factors. J Cell Biol 223: e202402046, 2024. doi:10.1083/jcb.202402046.
- Morena da Silva F, Lim S, Cabrera AR, Schrems ER, Jones RG, Rosa-Caldwell ME, Washington TA, Murach KA, Greene NP. The time-course of cancer cachexia onset reveals biphasic transcriptional disruptions in female skeletal muscle distinct from males. BMC Genomics 24: 374, 2023. doi:10.1186/s12864-023-09462-7.
- Kwak KS, Zhou X, Solomon V, Baracos VE, Davis J, Bannon AW, Boyle WJ, Lacey DL, Han HQ. Regulation of protein catabolism by muscle-specific and cytokine-inducible ubiquitin ligase  $E3\alpha$ -II during cancer cachexia. Cancer Res 64: 8193-8198, 2004. doi:10.1158/ 0008-5472.CAN-04-2102.
- Blondelle J, Biju A, Lange S. The role of cullin-RING ligases in striated muscle development, function, and disease. Int J Mol Sci 21: 7936, 2020. doi:10.3390/ijms21217936.
- Perez-Riverol Y, Bandla C, Kundu DJ, Kamatchinathan S, Bai J, Hewapathirana S, John NS, Prakash A, Walzer M, Wang S, Vizcaíno JA. The PRIDE database at 20 years: 2025 update. Nucleic Acids Res 53: D543-D553, 2025. doi:10.1093/nar/gkae1011.